Rapid Communications | Editors' Suggestion

Model-independent determination of the Migdal effect via photoabsorption

C.-P. Liu,[1,*] Chih-Pan Wu,[2,†] Hsin-Chang Chi,[1,‡] and Jiunn-Wei Chen[3,§]

[1]*Department of Physics, National Dong Hwa University, Shoufeng, Hualien 974301, Taiwan*
[2]*Département de physique, Université de Montréal, Montréal H3C 3J7, Canada*
[3]*Department of Physics, Center for Theoretical Physics, and Leung Center for Cosmology and Particle Astrophysics, National Taiwan University, Taipei 10617, Taiwan*

(Received 21 July 2020; accepted 4 November 2020; published 17 December 2020)

The Migdal effect in a dark-matter-nucleus scattering extends the direct search experiments to the sub-GeV mass region through electron ionization with sub-keV detection thresholds. In this paper, we derive a rigorous and model-independent "Migdal-photoabsorption" relation that links the sub-keV Migdal process to photoabsorption. This relation is free of theoretical uncertainties as it only requires the photoabsorption cross section as the experimental input. Validity of this relation is explicitly checked in the case of xenon with a state-of-the-art atomic calculation that is well benchmarked by experiments. The predictions based on this relation for xenon, argon, semiconductor silicon, and germanium detectors are presented and discussed.

DOI: 10.1103/PhysRevD.102.121303

I. INTRODUCTION

Direct searches for the weakly interacting massive particle (WIMP), one of the favorite dark matter (DM) candidates, has been making tremendous progress in recent years: in the mass range of $m_\chi \sim 10$–100 GeV,[1] the limits on its spin-independent scattering cross section off nucleon reach down to the range of $\sigma_n \lesssim 10^{-46} - 10^{-47}$ cm^2; in the mass range of 1–10 GeV, the limits are also improving, however, not as stringent as in the heavier case (see, e.g., Ref. [1] for a recent review). The obvious reason is a lighter WIMP has less kinetic energy so it is less probable to generate observable nuclear recoil (NR) events from WIMP-nucleus scattering. Ultimately, a detector's NR threshold cuts off any sensitivity to m_χ below a certain value, as seen in every WIMP exclusion plot.

To expand a direct detector's coverage of low-mass WIMPs, or more generically light dark matter (LDM), a recent proposal by Ibe *et al.* [2] that uses the so-called Migdal effect has attracted great interests. This effect, first noted by A. B. Migdal [3], refers to an inelastic exit channel in scattering off an atomic nucleus, where not only the atomic center of mass gets recoil (typically termed as NR), but also the intrinsic atomic electron state is excited or ionized. Unlike the elastic exit channel, the Migdal effect generates other electromagnetic signals in the form of ionized electrons and photons from atomic deexcitation or recombination, which are more energetic than NR hence is detectable. This novel DM detection mode has been applied to several experiments [4–10] and some of them give the current best limits on DM-nucleus interactions in the mass range below GeV. With detectors of larger size and longer data taking time, e.g., xenon-based XENONnT [11], LZ [12], and DARWIN [13]; argon-based DarkSide [14], DEAP [15], and ArDM [16]; or of lower threshold and better resolution, e.g., germanium-based EDELWEISS [17] and CDMS HVeV [18]; silicon-based SENSEI [19] and DAMIC [20], the Migdal effect will be a promising probe of hadrophilic LDM.

While detecting the Migdal effect is an experimental challenge, predicting its count rate is mostly a theoretical one [2,21–23]. For a relic sub-GeV LDM candidate, its kinetic energy is no bigger than a few keV, so the scattering process falls in the atomic scale. Proper understanding of such a sub-keV Migdal effect inevitably involves atomic physics. The lower the energy, the more pronounced many-body effects are expected. The complexity of many-body physics adds a new layer when detector media can no longer be treated as isolated atoms. This means at certain low-energy levels it will be necessary to take into account molecular or condensed-matter physics, depending on a detector's material phase. All these problems are highly nontrivial but essential.

To address the theory issues related to the Migdal effect, we first derive a relation that links the low-energy Migdal process to photoabsorption, which is exact at the long

*cpliu@mail.ndhu.edu.tw
†chih-pan.wu@umontreal.ca
‡hsinchang@gms.ndhu.edu.tw
§jwc@phys.ntu.edu.tw

[1]We use the natural units $\hbar = c = 1$ exclusively in this paper.

wavelength limit of photon and expected to work up to a few keV. The relation has two major advantages: it applies to all kinds of DM detectors in general, and is free of theoretical uncertainties because only photoabsorption cross section (experimentally measurable) is needed for input. To demonstrate the robustness of this relation, we study the case of xenon by applying a state-of-the-art atomic approach, the relativistic random phase approximation (RRPA), whose high precision has been demonstrated in Ref. [24]. Finally we use this relation to predict the Migdal effects in argon, silicon, and germanium detectors.

II. MIGDAL EFFECT

The transition operator and matrix element of a Migdal process has been derived in several ways, e.g., through a sudden approximation [25], nonrelativistic scattering with Galilean invariance [26] (for hydrogenlike systems), and relativistic scattering with full Lorentz covariance [2]. Because of the hierarchy between atomic, nuclear, electron mass, m_A, m_N, m_e, and atomic binding energy E_B: $m_A \approx m_N \gg m_e \gg E_B$, all derivations converge on the resulting Migdal matrix element

$$M_{FI} = \langle F | e^{-i\frac{m_e}{m_A}\vec{q}_A \cdot \sum_{i=1}^{Z} \vec{r}_i} | I \rangle, \tag{1}$$

where $\vec{q}_A$ is the three-momentum transfer to the atomic system; $\vec{r}_i$ the coordinate of the ith electron; $|I\rangle$ and $|F\rangle$ the atomic initial and final states in the intrinsic frame (i.e., with the center of mass motion being factored out), respectively.[2]

First, notice that the summation over all Z electron coordinates appears in the exponent, so the nth-order series expansion contains n-body operators, whose matrix elements are tedious to compute. By a naïve dimensional analysis: $|\vec{q}_A| \sim m_\chi v_\chi$ with DM velocity $v_\chi \sim 10^{-3}$; and $\langle \vec{r}_i \rangle \sim (Z_i m_e \alpha)^{-1}$ with Z_i being the effective charge seen by the ith electron and α the fine structure constant, one can define an atomic-shell-dependent expansion parameter $\epsilon_i = \frac{m_\chi}{m_A}\frac{v_\chi}{\alpha}\frac{1}{Z_i}$. In the case of xenon, $m_A \sim 120$ GeV, so $\epsilon_i \sim \frac{0.001}{Z_i}\frac{m_\chi}{\mathrm{GeV}}$ guarantees good convergence for sub-GeV DM even with a $Z_i = 1$ assumption. In reality, current xenon detector thresholds are a few keV, most Migdal events would be from inner-shell ionizations with Z_i surely larger than 1. Therefore, for LDM searches, the Migdal matrix element can be well-approximated by the leading-order term

$$M_{FI}^{(1)} = -i\frac{m_e}{m_A}\vec{q}_A \cdot \left\langle F \left| \sum_{i=1}^{Z} \vec{r}_i \right| I \right\rangle \equiv -i\frac{m_e}{m_A}\vec{q}_A \cdot \vec{D}_{FI}, \tag{2}$$

where $\vec{D}_{FI}$ is the familiar dipole matrix element.

[2]In this work, atomic states are treated relativistically, so the Migdal operator is a 4×4 diagonal matrix.

The energy deposition by DM in a Migdal process goes into two parts: one to the atomic center-of-mass kinetic energy (or the NR energy), E_R, and the other to the atomic discrete excitation or ionization, denoted as $E_r = E_F - E_I$ whit $E_{F(I)}$ the eigenenergy of the state $|F(I)\rangle$. To accommodate different DM detector's approaches in measuring the combinations of E_R and E_r, it is customary to cast the cross section in a double differential form

$$\frac{d\sigma}{dE_R dE_r} = \frac{m_e^2}{\mu_N^2 v_\chi^2}\tilde{\sigma}_N(q_A) E_R \overline{D_{FI}^2}, \tag{3}$$

where $\mu_N = m_N m_\chi/(m_N + m_\chi)$ is the reduced mass of the DM-nucleus system, and $\tilde{\sigma}_N$ the DM-nucleus cross section, which depends on $q_A = \sqrt{2 m_A E_R}$. The averaged dipole matrix element squared $\overline{D_{FI}^2}$ involves a summation of all allowed final states and an average of degenerate initial states.[3]

III. PHOTOABSORPTION AND ITS RELATION TO THE MIGDAL EFFECT

As seen from Eq. (3), the quantity $\overline{D_{FI}^2}$ is the critical piece of information that requires many-body calculations. Therefore, it is desirable to ask whether it can be extracted directly from experiments. Fortunately, photoabsorption provides the answer.

The full transition matrix element for photoabsorption takes the form

$$P_{FI} = \hat{\varepsilon} \cdot \left\langle F \left| \sum_{i=1}^{Z} \vec{\alpha}_i e^{i\vec{k}\cdot\vec{r}_i} \right| I \right\rangle \equiv \hat{\varepsilon} \cdot \vec{O}_{FI}, \tag{4}$$

where $\vec{k}$ and $\hat{\varepsilon}$ are the photon momentum and polarization vectors, and $\vec{\alpha}_i$ the 4×4 spatial Dirac matrix. By energy conservation, the photon energy $\omega = |\vec{k}| = E_r$ (the atomic recoil is negligible as $\omega \ll m_A$). The total cross section of photoabsorption is

$$\sigma_\gamma(E_r) = \frac{4\pi^2\alpha}{E_r}\overline{P_{FI}^2}, \tag{5}$$

where the same summation and average of states being applied to P_{FI} as in the case to D_{FI} (see the Appendix and Refs. [27,28] for details).

The standard procedure of calculating $\sigma_\gamma(E_r)$ starts by a multipole expansion of P_{FI} that yields the transverse electric, $T_J^{el}(kr)$, and transverse magnetic, $T_J^{mag}(kr)$, multipoles with $J = 1, 2, \ldots$ denoting the spherical multipolarity.

[3]Our choice of wave function normalization is $\langle E_I | E_{I'} \rangle = \delta_{II'}$ for bound states and $\langle E_F | E_{F'} \rangle = \delta(E_F - E_{F'})$ for continuum states.

At the long wavelength (LW) limit, i.e., $k\langle r\rangle \ll 1$ so that $e^{i\vec{k}\cdot\vec{r}} \to 1$, the transition matrix element is simplified to

$$\vec{O}_{FI}^{(E1)} = \left\langle F\left|\sum_{i=1}^{Z}\vec{\alpha}_i\right|I\right\rangle \equiv \vec{D}_{FI}^{(\mathrm{V})} = iE_r\vec{D}_{FI}. \tag{6}$$

This is the electric dipole ($E1$) approximation for photoabsorption, as the resulting atomic operator is a parity-odd dipole, either as $\vec{\alpha}_i$, usually termed as the velocity form (denoted by the superscript "V"), or $\vec{r}_i$, the length form. The equivalence of these two operators is established by the commutation relation $-i[\vec{r}_i, H] = \vec{\alpha}_i$. As a result, $\sigma_\gamma(E_r)$ can be approximated by

$$\sigma_\gamma(E_r) \xrightarrow[E1\ \text{approx}]{} 4\pi^2\alpha E_r\overline{D_{FI}^2}, \tag{7}$$

and the Migdal differential cross section can be cast into

$$\frac{d\sigma^{(\mathrm{MPA})}}{dE_R dE_r} = \frac{m_e^2}{\mu_N^2 v_\chi^2}\tilde{\sigma}_N(q_A)\frac{E_R}{E_r}\frac{\sigma_\gamma(E_r)}{4\pi^2\alpha}, \tag{8}$$

which we call the "Migdal-photoabsorption" (MPA) relation. This relation is powerful: it tells that as long as the photoabsorption cross section can be measured in a detector, the corresponding Migdal effect can be figured accordingly, and there is no need for theory input. In contrast, the relation proposed in Ref. [22] involves DM-electron scattering, which is yet to be detected.

While the derivation of the $E1$ approximation is straightforward, there are two points of particular importance from a theory viewpoint. First, at the LW limit, all the so-called retardation effects from $e^{i\vec{k}\cdot\vec{r}} - 1$ are ignored. They are grouped into higher-rank spherical multipoles or higher-order corrections (in powers of k^2r^2) to spherical multipoles of a given rank.

Second, the equivalence between the dipole operators in the velocity and length forms, manifested here by a simple commutation relation, has a deeper connection to the gauge invariance of electromagnetism. As first noted by Siegert [29], the transverse electric multipole operators can be related by current conservation to the charge multipole operators at the LW limit. However, the equivalence at the matrix-element level has an additional requirement that the wave functions are energy eigenstates, i.e., $H|F(I)\rangle = E_{F(I)}|F(I)\rangle$. For most many-body calculations that only approximate the true eigenstates, the breaking of gauge invariance, e.g., $\vec{D}_{FI}^{(\mathrm{V})} \neq \vec{D}_{FI}$, is quite commonly seen. Therefore, adopting many-body approaches that preserve gauge invariance, such as (R)RPA [30],[4] is preferred. Conversely, the degree of broken gauge invariance can serve as a robustness test of a many-body calculation. In atomic physics, this is usually done with two different forms of T_J^{el}, one in the Coulomb gauge and the other the "length gauge" [31].

[4]In the same paper [30], the most commonly used Hartree-Fock method is shown to violate gauge invariance.

IV. CASE STUDY OF XENON

In Fig. 1, the experimental data for xenon photoabsorption, compiled from Refs. [32–36], are compared with several theoretical calculations. The agreement between the RRPA curve, taken from Ref. [24] using operators in the length gauge, shows that our atomic approach can handle many-body excited states properly. In this work, we carry out two additional calculations: one with the $E1$ approximation, i.e., Eq. (7), and the other with operators in the Coulomb gauge. As shown in the central panel, the $E1$ approximation works very well up to 1 keV with all higher-order corrections still kept at a level below 1%. This justifies the basic assumption underlying the MPA relation: the averaged dipole matrix element squared $\overline{D_{FI}^2}$ in the sub-keV Migdal process can be reliably extracted from photoabsorption measurements. In the bottom panel, the nontrivial property of gauge invariance in many-body calculations is clearly shown to be preserved by the RRPA approach.

The FAC results are obtained by running a built-in module in the "Flexible Atomic Code" package that calculates photoionization cross sections directly [37]. As the comparison shows, the FAC code does a reasonably good job for $E_r \gtrsim 200$ eV in general, but at lower energies, it does not perform well, and errors at some points are quite large. By construct, the FAC package is mainly designed for highly ionized atoms and built with focus on efficiency

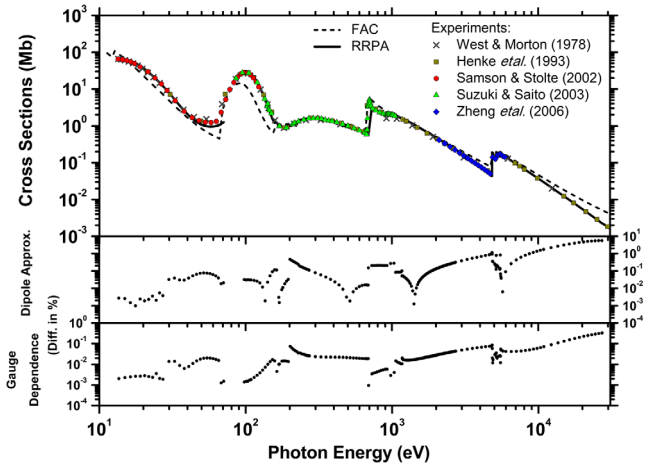

FIG. 1. (Top panel) xenon photoabsorption cross section from experiments and atomic calculations of RRPA with the length-gauge operators and the FAC code. Also shown are the percentage differences by using the $E1$ approximation (central panel) and from using the Coulomb gauge operators (bottom panel) in the same RRPA routine.

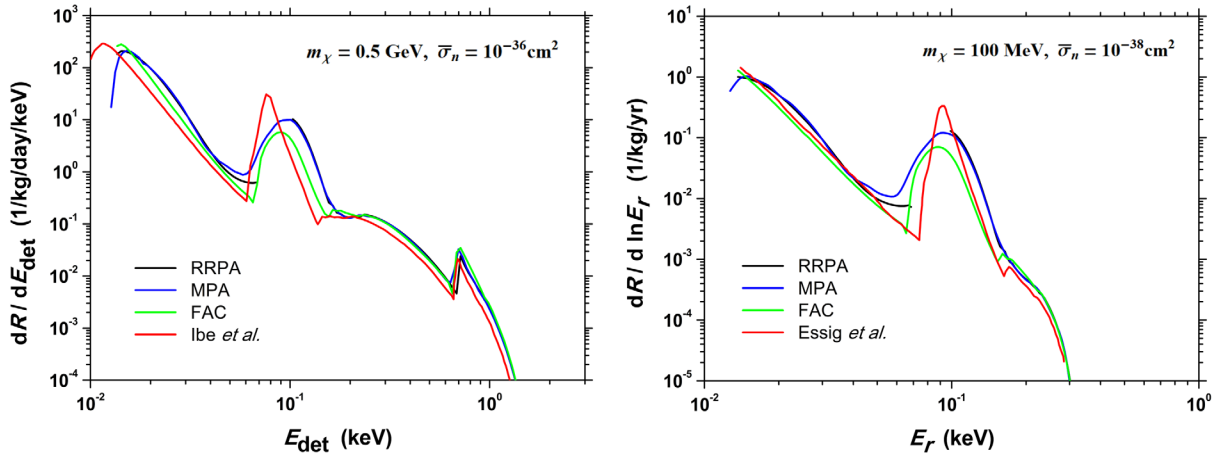

FIG. 2. Differential count rates $\frac{dR}{dE_{\rm det}}$ (left) and $\frac{dR}{d\ln E_r}$ (right) of the Migdal effect in xenon detectors by the spin-independent, isoscalar, DM-nucleon contact interaction (with cross section $\bar{\sigma}_n$) predicted by (i) RRPA, (ii) MPA relation, (iii) FAC, and (iv) Ref. [2] (left) and Ref. [22] (right).

instead of accuracy. Therefore, its many-body approach is solving a prescribed form of averaged one-body potential (in this sense, not an *ab inito* approach) self-consistently, and leads to a picture that all electrons act like independent particles, which is unrealistic at low energies. Another noteworthy point is for $E_r \gtrsim 1$ keV, FAC has the tendency to over-predict when E_r gets away from edge energies. This is because the transition operators being adopted, except $T_1^{\rm mag}$, are nonrelativistic, and contributions from all subleading orders in k^2r^2 are missing.

For prediction of Migdal count rates, we follow the same procedures as in Refs. [2] and [22]. In the former case, the observable energy $E_{\rm det}$ is a sum of E_r and $q_{\rm nr}E_R$ with $q_{\rm nr}$ the NR quenching factor, and the differential count rate is

$$\frac{dR}{dE_{\rm det}} = n_\chi N_T \int dE_R \int dE_r \delta(E_{\rm det} - q_{\rm nr}E_R - E_r) \times \tilde{\sigma}_N(q_A) E_R \overline{D_{FI}^2} \eta(v_{\rm min}). \quad (9)$$

For the latter case, the observable energy is E_r and the differential count rate is simply

$$\frac{dR}{dE_r} = n_\chi N_T \frac{m_e^2}{\mu_N^2} \overline{D_{FI}^2} \int dE_R \tilde{\sigma}_N(q_A) E_R \eta(v_{\rm min}), \quad (10)$$

where n_χ is the local DM number density, N_T the number of target atoms, and the η function results from the $1/v_\chi$ factor averaged with the DM velocity spectrum [38], and depends on the minimum DM velocity $v_{\rm min} = (m_N E_R + \mu_N E_r)/(\mu_N\sqrt{2m_N E_R})$ that guarantees energy deposition of $E_R + E_r$ is possible.

In Fig. 2, we plot four sets of count rate predictions assuming a contact, spin-independent, isoscalar DM-nucleus interaction so that $\tilde{\sigma}_N = A^2\mu_N^2\mu_n^{-2}\bar{\sigma}_n$ with μ_n being the DM-nucleon reduced mass and $\bar{\sigma}_n$ the DM-nucleon cross section: the black line is by direct computation of Eq. (3) using RRPA; the blue (green) line is obtained by the MPA relation with $\sigma_\gamma(E_r)$ taken from data (FAC). The nice agreement between RRPA and MPA is not only a justification to the applicability of the MPA relation, but also a theory-experiment double confirmation of the results. The difference between our results from the ones of Refs. [2,22] are most likely originated from different atomic approaches. Generally speaking, mean field methods can give good results of ground state properties and wave functions, but their applicability to excited states can be problematic. Note that Ref. [2] used the FAC package differently from what we do. The authors adopted the picture that the atomic excited states are purely one-particle-one-hole excitations (because the leading-order Migdal operator is one-body) from the ground state. This independent particle picture ignores not only the residual two-body correlation, but also the fact that atomic mean field varies with electronic configuration. The FAC package takes into account the latter aspect by diagonalizing the atomic Hamiltonian in the model space of a given problem. The resulting wave functions are configuration mixed, i.e., not in form of a single Slater determinant. This explains why the FAC results are closer to our RRPA results than Ref. [2].

V. APPLICATIONS TO ARGON, SILICON, AND GERMANIUM DETECTORS

Using the MPA relation, we combine in Fig. 3 the predicted count rates for xenon, argon, semiconductor silicon, and germanium detectors. For $E_r \geq 10$ eV, the measured photoabsorption data are taken from Ref. [33] along with semiempirical fitting; for semiconductor silicon and germanium in 1 eV $< E_r <$ 10 eV, data are taken with intrinsic bulk samples at room temperature and given in Refs. [39,40].

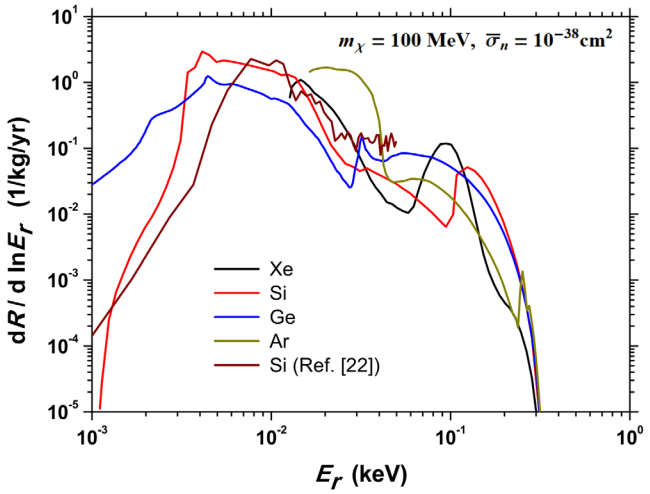

FIG. 3. Differential count rates $\frac{dR}{d\ln E_r}$ for xenon, argon, semiconductor silicon, and germanium detectors.

Similar to the xenon case which is carefully examined in the last section, the argon prediction should be robust, unlike the large theoretical uncertainties assigned in Ref. [41] based on the atomic calculation of Ref. [2]. However, it is the applications to low-threshold semiconductors that the MPA relation fully exhibit its predictive power.

It is well-known that the photoelectric effect dominates the photoabsorption process of a semiconductor above its band gap, which is on the order of eV. Take silicon as an example, the fundamental band gap is ∼1.2 eV. However, because this gap is indirect, the first big absorption edge shows at a higher energy ∼3 eV. This peak is due to a direct transition from a valence to a conduction band of equal pseudomomentum. As an eV-scale photon has a much smaller momentum, the validity of the $E1$ approximation[5] and the MPA relation is justified. Our predicted count rate for silicon exhibits all the essential characters just mentioned, but differs from Ref. [22]. Since the latter is done by extrapolating a crystal form factor at high momentum to almost-zero momentum, the dipole scaling relation deserves further confirmation. On the other hand, photoabsorption of a semiconductor device also depends on its design, working temperature, dopant concentration etc. Therefore, for experiments like DAMIC [44] and SENSEI [45] whose detectors are silicon CCDs with n-type substrate and p-type channel and operated at $\sim 100K$, their Migdal count rates should differ from the red curve in Fig. 3. The detailed theory calculations for these real cases are formidable, but with the MPA relation, they can be bypassed through photoabsorption measurements.

Also impressively, the MPA relation provides a reliable germanium prediction in the energy range of 1–80 eV. According to our previous study of atomic germanium [46,47], the MCRRPA method (the RRPA with multiconfiguration required for open-shell atoms), though sophisticated enough, does not work satisfactorily in this energy range because of the crystal effects. Now, it is no longer an obstacle, and the experimental analyses, such as being done by EDELWEISS [7] and CDEX [8], can include these shells, which have dominant contributions for $E_r < 100$ eV. Another significant feature is that the germanium detector can be very sensitive to the Migdal effect at extremely low energy, because of its specially large photoabsorption coefficient in $E_r = 1$–3 eV. Both CDMS HVeV [18] and EDELWEISS [17] recently demonstrate their extremely-low-threshold capability at 1 eV. According to the plot, the Migdal count rate can be three-order-of-magnitude bigger than in a silicon detector, assuming equal exposure mass time.

It should also be pointed out that different detectors complement one another, thanks to the rich atomic structure. At each photoabsorption peak, the cross section and the resulting Migdal rate can receive an substantial boost. This not only enhances the sensitivity but also provides smoking gun signatures.

The high energy limit to which the MPA relation works depends on the validity of the $E1$ approximation in photoabsorption. For the four considered cases with varied atomic number and mass, we explicitly check the corrections are all below 1% up to photon energy of a few keV. Therefore, the MPA relation should be safely applicable to the Migdal effects generated by sub-GeV DM particles in galactic halo, whose kinetic energies are less than 1 keV.

VI. CONCLUSION

The Migdal effect has been a powerful search mode for hadrophilic, sub-GeV light dark matter. With modern technologies pushing detector thresholds lower and lower, our range of light dark matter searches will expand further. The "Migdal-photoabsorption" relation we derived in this work is based on general principles and only requires photoabsorption measurements as input. It thus provides predictions that have no uncertainties from many-body calculations. Though we only consider xenon, argon, semiconductor silicon, and germanium detectors as examples, it certainly can be applied to other novel low-threshold detectors.

ACKNOWLEDGMENTS

This work is supported in part under Grants No. 108-2112-M-259-003 (C. P. L.), No. 108-2112-M-002-003-MY3 (J. W. C.) from the Ministry of Science and Technology, No. 2019-20/ECP-2 from the National Center for Theoretical Sciences, and Kenda Foundation (J. W. C.) of Taiwan; and the Canada First Research Excellence Fund through the Arthur B. McDonald Canadian Astroparticle Physics

[5]We note that the $E1$ approximation is widely adopted in theoretical calculations of photoabsorption in semiconductors with good agreement with experiments, see, e.g., Refs. [42,43].

Research Institute (C. P. W.). We also thank Chung-Chun Hsieh and Mukesh K. Pandey for early participation.

APPENDIX: PHOTOABSORPTION CROSS SECTION

Starting from the Hamiltonian of a free, relativistic electron

$$H_0 = \vec{\alpha}\cdot\vec{p} + \beta m_e,$$

where $\vec{\alpha}$ and β are the conventional Dirac matrices, its interaction with a radiation field $\vec{A}$ (in radiation gauge, the scalar potential is fixed to zero) can be easily obtained by the minimal coupling

$$V = e\vec{\alpha}\cdot\vec{A},$$

with the coupling constant $e = \sqrt{4\pi\alpha}$. In photoabsorption, a massless photon of momentum $\vec{k}$ (energy $\omega = |\vec{k}|$) and polarization vector $\hat{\varepsilon}$, whose wave function

$$\langle\vec{r}|\vec{k},\hat{\varepsilon}\rangle = \frac{1}{\sqrt{2\omega}}e^{i\vec{k}\cdot\vec{r}},$$

is annihilated and the target state changes from $|I\rangle$ to $|F\rangle$. The first-order transition matrix element

$$V_{FI} = \langle F|V|I;\vec{k},\hat{\varepsilon}\rangle = \frac{e}{\sqrt{2\omega}}\langle F|\vec{\alpha}e^{i\vec{k}\cdot\vec{r}}|I\rangle\cdot\hat{\varepsilon}.$$

According to the Fermi golden rule, the differential cross section

$$d\sigma_\gamma = 2\pi|V_{FI}|^2\delta(E_F - E_I - \omega)d\Omega_F.$$

To obtain the total cross section, the summation over the final-state phase space Ω_F includes the one of E_F, which leads to the energy conservation $E_F = E_I + \omega$, and all the other quantum numbers, collectively labeled by γ_F. For an unpolarized target, there is another sum over the degenerate quantum numbers, collectively labeled by δ_I, divided by the number of degeneracy d_I. As a result,

$$\sigma_\gamma = \frac{4\pi^2\alpha}{E_F - E_I}\sum_{\gamma_F}\sum_{\delta_I}\frac{1}{d_I}|\langle F|\vec{\alpha}e^{i\vec{k}\cdot\vec{r}}|I\rangle\cdot\hat{\varepsilon}|^2,$$

and this is Eq. (5) in the main text.

The electric dipole approximation, $e^{i\vec{k}\cdot\vec{r}} \to 1$, gives rise to a simple dipole operator $\vec{\alpha}$ in the velocity form. The transformation of $\vec{\alpha}$ to a length-form dipole $\vec{r}$ is based on the commutation relation

$$\vec{\alpha} = -i[\vec{r}, \vec{\alpha}\cdot\vec{p} + \beta m_e + V_{ee} + V_{eN}].$$

This is valid when electron-electron and electron-nucleus interactions have no momentum-dependent components (for example, purely Coulomb), which indeed is a starting point for most many-body studies of atoms, molecules, and condensed matter.

[1] P. A. Zyla *et al.* (Particle Data Group), Prog. Theor. Exp. Phys. (**2020**), 083C01.
[2] M. Ibe, W. Nakano, Y. Shoji, and K. Suzuki, J. High Energy Phys. 03 (2018) 194.
[3] A. B. Migdal, Zh. Eksp. Teor. Fiz. **9**, 1163 (1939).
[4] M. J. Dolan, F. Kahlhoefer, and C. McCabe, Phys. Rev. Lett. **121**, 101801 (2018).
[5] M. Kobayashi *et al.* (XMASS Collaboration), Phys. Lett. B **795**, 308 (2019).
[6] D. Akerib *et al.* (LUX Collaboration), Phys. Rev. Lett. **122**, 131301 (2019).
[7] E. Armengaud *et al.* (EDELWEISS Collaboration), Phys. Rev. D **99**, 082003 (2019).
[8] Z. Liu *et al.* (CDEX Collaboration), Phys. Rev. Lett. **123**, 161301 (2019).
[9] E. Aprile *et al.* (XENON Collaboration), Phys. Rev. Lett. **123**, 241803 (2019).
[10] L. Barak *et al.* (SENSEI Collaboration), Phys. Rev. Lett. **125**, 171802 (2020).
[11] E. Aprile *et al.* (XENON Collaboration), arXiv:2007.08796.
[12] D. Akerib *et al.* (LZ Collaboration), Nucl. Instrum. Methods Phys. Res., Sect. A **953**, 163047 (2020).
[13] J. Aalbers *et al.* (DARWIN Collaboration), J. Cosmol. Astropart. Phys. 11 (2016) 017.
[14] C. Aalseth *et al.*, Adv. High Energy Phys. **2015**, 541362 (2015).
[15] P.-A. Amaudruz *et al.* (DEAP-3600 Collaboration), Astropart. Phys. **108**, 1 (2019).
[16] J. Calvo *et al.* (ArDM Collaboration), J. Cosmol. Astropart. Phys. 03 (2017) 003.
[17] Q. Arnaud *et al.* (EDELWEISS Collaboration), Phys. Rev. Lett. **125**, 141301 (2020).
[18] R. Agnese *et al.* (SuperCDMS Collaboration), Phys. Rev. Lett. **121**, 051301 (2018); **122**, 069901(E) (2019).
[19] O. Abramoff *et al.* (SENSEI Collaboration), Phys. Rev. Lett. **122**, 161801 (2019).
[20] A. Aguilar-Arevalo *et al.* (DAMIC Collaboration), Phys. Rev. Lett. **123**, 181802 (2019).
[21] N. F. Bell, J. B. Dent, J. L. Newstead, S. Sabharwal, and T. J. Weiler, Phys. Rev. D **101**, 015012 (2020).

[22] R. Essig, J. Pradler, M. Sholapurkar, and T.-T. Yu, Phys. Rev. Lett. **124**, 021801 (2020).
[23] D. Baxter, Y. Kahn, and G. Krnjaic, Phys. Rev. D **101**, 076014 (2020).
[24] J.-W. Chen, H.-C. Chi, C.-P. Liu, and C.-P. Wu, Phys. Lett. B **774**, 656 (2017).
[25] L. D. Landau and E. M. Lifshitz, *Quantum Mechanics (Non-relativistic Theory)* (Butterworth Heinemann, Oxford, 1991).
[26] J.-W. Chen, H.-C. Chi, C. P. Liu, C.-L. Wu, and C.-P. Wu, Phys. Rev. D **92**, 096013 (2015).
[27] H. A. Bethe and E. E. Salpeter, *Quantum Mechanics of One- and Two-Electron Atoms* (Academic Press, New York, 1957).
[28] V. B. Berestetskii, E. M. Lifshitz, and L. P. Pitaevskii, *Quantum Electrodynamics*, 2nd ed. (Pergamon Press, Oxford, 1982).
[29] A. Siegert, Phys. Rev. **56**, 750 (1939).
[30] D. L. Lin, Phys. Rev. A **16**, 600 (1977).
[31] I. P. Grant, J. Phys. B **7**, 1458 (1974).
[32] J. B. West and J. Morton, At. Data Nucl. Data Tables **22**, 103 (1978).
[33] B. L. Henke, E. M. Gullikson, and J. C. Davis, At. Data Nucl. Data Tables **54**, 181 (1993).
[34] J. Samson and W. Stolte, J. Electron Spectrosc. Relat. Phenom. **123**, 265 (2002).
[35] I. H. Suzuki and N. Saito, J. Electron Spectrosc. Relat. Phenom. **129**, 71 (2003).
[36] L. Zheng, M. Cui, Y. Zhao, J. Zhao, and K. Chen, J. Electron Spectrosc. Relat. Phenom. **152**, 143 (2006).
[37] M. F. Gu, Can. J. Phys. **86**, 675 (2008).
[38] J. Lewin and P. Smith, Astropart. Phys. **6**, 87 (1996).
[39] S. M. Sze, *Physics of Semiconductor Devices* (John Wiley and Sons, N.Y., 1981).
[40] H. R. Philipp and E. A. Taft, Phys. Rev. **113**, 1002 (1959).
[41] G. Grilli di Cortona, A. Messina, and S. Piacentini, arXiv:2006.02453.
[42] S. Botti, Phys. Rev. B **69**, 155112 (2004).
[43] C.-Y. Tsai, J. Appl. Phys. **123**, 183103 (2018).
[44] A. Aguilar-Arevalo *et al.* (DAMIC Collaboration), J. Instrum. **10**, P08014 (2016).
[45] J. Tiffenberg, M. Sofo-Haro, A. Drlica-Wagner, R. Essig, Y. Guardincerri, S. Holland, T. Volansky, and T.-T. Yu (SENSEI Collaboration), Phys. Rev. Lett. **119**, 131802 (2017).
[46] J.-W. Chen, H.-C. Chi, K.-N. Huang, C.-P. Liu, H.-T. Shiao, L. Singh, H. T. Wong, C.-L. Wu, and C.-P. Wu, Phys. Lett. B **731**, 159 (2014).
[47] J.-W. Chen, H.-C. Chi, K.-N. Huang, H.-B. Li, C.-P. Liu, L. Singh, H. T. Wong, C.-L. Wu, and C.-P. Wu, Phys. Rev. D **91**, 013005 (2015).